

Nitrous oxide dimer: A new potential energy surface and rovibrational spectrum of the nonpolar isomer

Richard Dawes,^{1,a)} Xiao-Gang Wang,^{3,b)} Ahren W. Jasper,^{2,c)} and Tucker Carrington, Jr.^{3,d)}

¹Missouri University of Science and Technology, Rolla, Missouri 65401, USA

²Combustion Research Facility, Sandia National Laboratories, P.O. Box 969, Livermore, California 94551, USA

³Department of Chemistry, Queen's University, Kingston, Ontario K7L 3N6, Canada

(Received 10 August 2010; accepted 9 September 2010; published online 4 October 2010)

The spectrum of nitrous oxide dimer was investigated by constructing new potential energy surfaces using coupled-cluster theory and solving the rovibrational Schrödinger equation with a Lanczos algorithm. Two four-dimensional (rigid monomer) global *ab initio* potential energy surfaces (PESs) were made using an interpolating moving least-squares (IMLS) fitting procedure specialized to describe the interaction of two linear fragments. The first exploratory fit was made from 1646 CCSD(T)/3ZaP energies. Isomeric minima and connecting transition structures were located on the fitted surface, and the energies of those geometries were benchmarked using complete basis set (CBS) extrapolations, counterpoise (CP) corrections, and explicitly correlated (F12b) methods. At the geometries tested, the explicitly correlated F12b method produced energies in close agreement with the estimated CBS limit. A second fit to 1757 data at the CCSD(T)-F12b/VTZ-F12 level was constructed with an estimated fitting error of less than 1.5 cm^{-1} . The second surface has a global nonpolar O-in minimum, two T-shaped N-in minima, and two polar minima. Barriers between these minima are small and some wave functions have amplitudes in several wells. Low-lying rovibrational wave functions and energy levels up to about 150 cm^{-1} were computed on the F12b PES using a discrete variable representation/finite basis representation method. Calculated rotational constants and intermolecular frequencies are in very close agreement with experiment.

© 2010 American Institute of Physics. [doi:10.1063/1.3494542]

I. INTRODUCTION

A number of spectroscopic studies of the nitrous oxide dimer (NNO)₂ have appeared in the literature since 1978,¹⁻⁷ with the recent observation of a new polar isomer sparking renewed interest.⁸⁻¹³ Motivated in part by analogy to the OCS and CO₂ dimers, several stable isomers have been predicted, including nonpolar, polar, and “T-shaped” conformers.^{5,8,14} Infrared and microwave spectra have only been assigned to nonpolar slipped antiparallel and polar skewed-parallel isomers. Dehghani *et al.*⁸ emphasized the need for a good *ab initio* intermolecular potential energy surface to aid in interpreting experimental results. In this paper we present a new, highly accurate, potential energy surface and rovibrational energy levels computed on it by solving the rovibrational Schrödinger equation with a product basis and the Lanczos algorithm.

In a previous theoretical study of the spectroscopy of (NNO)₂, Berner *et al.*¹⁵ determined stationary points and reported harmonic frequencies for various isomers using Dunning's augmented double-zeta basis¹⁶ (AVDZ) and the CCSD coupled cluster method. They performed additional single point calculations including triples perturbatively with an augmented triple-zeta basis (CCSD(T)/AVTZ), but did not fit

a surface. These calculations were compared with density functional theory (PW91) and Møller–Plesset perturbation theory (MP2, MP3, and MP4), and the lower-level methods were shown to be unreliable for (NNO)₂. Although anharmonicity and coupling are important for (NNO)₂ it is possible, surprisingly, to extract useful information from frequency shifts. For example, the difference between the calculated shifts for two bands in the dimer spectrum associated with the ν_1 monomer fundamental band aid in the assignment of the experimental spectrum. Their best estimate of the well depth of the nonpolar global minimum D_e (598 cm^{-1}) was based on a counterpoise corrected CCSD(T)/AVTZ//CCSD/AVDZ calculation and was assigned considerable uncertainty (200 cm^{-1}). The stability of a “T-shape N-in” isomer was found to be extremely sensitive to the level of theory.

To understand the spectroscopy of (NNO)₂ it is important to use an *ab initio* method that is capable of correctly computing the depths and shapes of the wells and the barrier heights, and it is also essential to account for coupling and anharmonicity when calculating the spectrum. The potential energy surface (PES) of (NNO)₂ has multiple wells separated by superable barriers. Many wave functions are so delocalized that it is not possible to associate all bands with a single well. To compute such states one needs high quality *ab initio* points, a good potential, and accurate solutions of the rovibrational Schrödinger equation.

In this paper we present a careful analysis of the accuracy of various *ab initio* methods for (NNO)₂, including

^{a)}Electronic mail: dawesr@mst.edu

^{b)}Electronic mail: xgwang.dalian@gmail.com

^{c)}Electronic mail: ajasper@sandia.gov.

^{d)}Electronic mail: tucker.carrington@queensu.ca.

CCSD(T) and explicitly correlated F12 methods with several basis sets and basis set extrapolation schemes. Analytic four-dimensional (4D) intermolecular PESs were constructed based on *ab initio* data using a specialized version of the interpolating moving least-squares (IMLS) fitting procedure. Two analytic IMLS PESs were developed. The PESs are accurate up to about 5200 cm⁻¹ above the dissociation energy and therefore reliably characterize all the stable isomers. First, a CCSD(T)/3ZaP PES was obtained to facilitate exploration of the van der Waals (vdW) region. The critical geometries on the CCSD(T)/3ZaP PES were used to test several high level *ab initio* methods, basis sets, and extrapolation schemes. A second quantitative CCSD(T)-F12b/VTZ-F12 PES was obtained based on these evaluations. The second PES was used to obtain low-lying solutions of the rovibrational Schrödinger equation corresponding to the nonpolar O-in isomer. Calculated rotational constants and intermolecular frequencies are compared with experiment.

II. IMLS PES FITTING

To construct a PES one must compute electronic energies at a set of points and then adjust parameters of a function so that the function either nearly passes through the points (fitting) or exactly passes through the points (interpolation). Various fitting methods have been proposed.¹⁷⁻²² It has been previously demonstrated that the IMLS fitting method is an effective tool for obtaining PESs with subwavenumber fitting error for several triatomics.²³⁻²⁵ In this paper we introduce and apply a refined version of the IMLS procedure. In principle the IMLS idea is general; however, vdW systems are especially difficult because a large region of configuration space with multiple local minima is accessible. The full range of the angular coordinates must be described and motion in the intermonomer coordinate is of large amplitude. At any geometry, \vec{r} , the IMLS potential is a weighted sum of local fits,

$$V(\vec{r}) = \frac{\sum_j w_j(\vec{r}) V_j(\vec{r})}{\sum_j w_j(\vec{r})}, \quad (1)$$

where the local fits $V_j(\vec{r})$ are expressed in some basis B_k ,

$$V_j(\vec{r}) = c_{j,0} + \sum_k c_{j,k} B_k(\vec{r}). \quad (2)$$

Each local fit j is centered at \vec{r}_j , which is the location of the j th *ab initio* data point used to fit the surface. A separate set of $(c_{j,k})$ is optimized, by doing a weighted least-squares fit, at each point. The efficiency of the IMLS fit depends on the choice of coordinates, basis functions, *ab initio* geometries, and the weight function $w_j(\vec{r})$ [used both in Eq. (1) and for making the local weighted least-squares fits], which in turn depends on a distance metric, as discussed below. The coordinates chosen for fitting the PES are defined in Fig. 1(a).

For characterization of the PESs, and to describe isomerization between planar isomers, we also make use of dis- and conrotatory coordinates X and Y [Eq. (3)]. X and Y are conveniently defined in terms of angles with direction²⁶ [$\tilde{\theta}_1$ and $\tilde{\theta}_2$, Fig. 1(b)]. To facilitate comparisons we adopt the ranges used by Berner *et al.*¹⁵ where $\tilde{\theta}_1 \in [-4\pi/3, 2\pi/3]$ and $\tilde{\theta}_2$

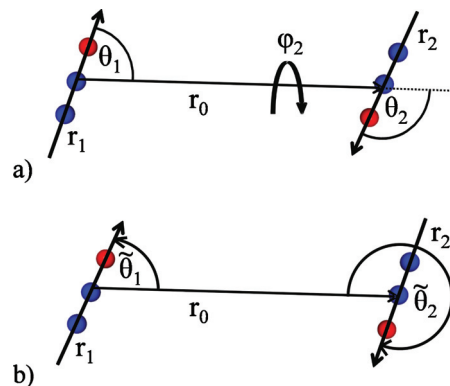


FIG. 1. Coordinates used to define dimer geometries. (a) Length of \mathbf{r}_0 , center-of-mass separation, angles of NNO-vectors (\mathbf{r}_1 and \mathbf{r}_2) with respect to \mathbf{r}_0 (θ_1 and θ_2), and torsional angle from \mathbf{r}_1 to \mathbf{r}_2 around \mathbf{r}_0 (ϕ_2). (b) Directional angles (with tilde) used to define con- and disrotatory coordinates [Eq. (3)] for planar structures.

$\in [-2\pi/3, 4\pi/3]$. The disrotatory coordinate X describes the out-of-phase motion with one monomer rotating counterclockwise while the other rotates clockwise. The conrotatory coordinate Y describes the concerted in-phase motion of both monomers rotating in either a clockwise or counterclockwise direction,

$$X = (\tilde{\theta}_1 + \tilde{\theta}_2)/2, \quad (3)$$

$$Y = (\tilde{\theta}_1 - \tilde{\theta}_2)/2.$$

The range of ϕ_2 is $[0, 2\pi]$, but because $V_j(\vec{r})$ is an even function of ϕ_2 , it is only necessary to use values between 0 and π .

Due to the difficulties cited above, the basis functions are chosen carefully. The basis functions we use are

$$B_k(r_0, \theta_1, \theta_2, \phi_2) = (-1)^{m_2} \exp(-\alpha r_0)^i \Theta_{L_1}^{m_2}(\theta_1) \times \Theta_{L_2}^{m_2}(\theta_2) \cos(m_2 \phi_2), \quad (4)$$

where k is a composite basis function index representing i , L_1 , L_2 , and m_2 . These functions are commonly used for fitting PESs for vdW systems with linear fragments,²⁷⁻³¹ but usually one set of functions is used to fit the entire potential. With IMLS we use many such sets to make local fits, one for each \vec{r}_j point. The range parameter α in the radial basis is fixed at $\alpha = 1.0 \text{ \AA}^{-1}$. The maximum radial power i was 6, and L_{\max} for the associated Legendre polynomials was also 6. The maximum value of the sum of L_1 and L_2 was limited to L_{\max} , and $m_2 \leq \min(L_1, L_2)$. These choices result in a total of 301 basis functions (at each local expansion point), including the constant. In other approaches where a single basis expansion is used, much larger values of $L_{\max} (> 6)$ are required. This in turn requires many *ab initio* points (quadrature points) to determine the coefficients. In some cases, accuracy in one part of the angular range is favored by damping the relative weight of points in another region; this reduces the number of required *ab initio* points.^{29,30} The present use of local expansions allows an accurate fit to be obtained with $L_{\max} = 6$.

The local fits are connected using a weight function so

that the IMLS potential passes through each of the *ab initio* points (with an error ε) and smoothly interpolates between them. The weight function is

$$w_j(\vec{r}) = \frac{\exp\left(-\left(\frac{d(\vec{r}_j, \vec{r})}{\rho(\vec{r}_j)}\right)^2\right)}{\left(\frac{d(\vec{r}_j, \vec{r})}{\rho(\vec{r}_j)}\right)^p + \varepsilon}. \quad (5)$$

In this application, $p=4$ and $\varepsilon=10^{-14}$ while the distance was determined using the distance metric

$$d(\vec{r}_j, \vec{r})^2 = ((r_0)_j - r_0)^2 + c^2[(\theta_{j,1} - \theta_1)^2 + (\theta_{j,2} - \theta_2)^2 + \sqrt{\sin(\theta_{j,1})\sin(\theta_1)\sin(\theta_{j,2})\sin(\theta_2)}((\varphi_2)_j - \varphi_2)^2]. \quad (6)$$

The form of the distance metric [Eq. (6)] is important for interpolation in these coordinates and requires thought because near $\theta_k=0$ or $\theta_k=\pi$ a small change in the shape may correspond to a large change in the value of φ_2 . Therefore, when assessing the similarity of two shapes one of which has θ_k close to 0 or π , it is important that φ_2 values not play an exaggerated role. The distance metric we use makes the measured distance between points differing significantly only in φ_2 and having θ_k close to 0 or π small, thus allowing smooth and continuous interpolation across the boundary at which φ_2 becomes undefined. The scaling factor ($c=2.315$ Å/rad) is chosen based on the length of the monomer fragments to put distance and angular displacements on an equal footing. Variation of the torsional coordinate is reflected in the distance metric as the arc length described by the exterior atoms of the linear monomers (becoming a small precession for small values of θ_1 and θ_2). The local data density parameter $\rho(\vec{r}_j)$ in Eq. (5) is the distance to the 20th nearest neighbor [as evaluated with Eq. (6)] from data point j .

The local expansion coefficients are determined at each *ab initio* point by a weighted linear least-squares fit using the LAPACK (Ref. 32) linear algebra routine DGELSS. Although the final potential is accurate globally, the local expansions $V_j(\vec{r})$ are only accurate close to \vec{r}_j . This behavior is ensured by the weight function, which weights the contribution of the *ab initio* data in the least-squares determinations of the expansion coefficients. The weight function is sharply peaked to ensure that the IMLS potential is interpolative and therefore only points close to \vec{r}_j have significant weights. The condition number (the ratio of the largest and smallest singular values) of the design matrix for the local fit $V_j(\vec{r})$ can be large, which can result in numerical instabilities in the determination of the expansion coefficients. These numerical instabilities do not affect the accuracy of the fitted potential at the *ab initio* data points but may slightly degrade the quality of the interpolated fit. One solution to this problem is to replace, when solving the linear equations, reciprocals of small singular values with zero. This corresponds to using a basis of linear combinations of the original basis functions and retaining only those linear combinations that are well determined. Rather than discarding reciprocals of singular values that are smaller than some fixed threshold, we determine the threshold at each expansion point by considering

the accuracy of the fitted local expansion. Specifically, the number of retained singular values is reduced until $\sqrt{\sum_{jp} w_j(\vec{r}_{jp}) [E(\vec{r}_{jp}) - V_j(\vec{r}_{jp})]^2}$ increases by 10%, where $E(\vec{r}_{jp})$ is the *ab initio* energy at a neighboring point jp . Note that the number of discarded singular values depends on geometry and on the number of *ab initio* points being fit. This is sensible because as *ab initio* data are added the number of well-determined linear combinations *does* change. We call our procedure *dynamic conditioning*. Tests indicate that removing small singular values in this fashion improves the fitting error, at test points not included in the fit, for the full potential [Eq. (1)] by roughly 30% (relative to use of a small fixed threshold).

The IMLS PESs were constructed by adding sets of *ab initio* data at geometries designed to most efficiently reduce the fitting error. Each fit was initiated with 500 *ab initio* data distributed throughout the vdW region with a probability distribution that favored small r_0 values. Our automated surface growing procedure based on the difference between trial fits using different fitting bases has been described before.²⁵ For (NNO)₂ the two trial fits are with a basis of 301 functions [$i_{\max}=6$, $L_{\max}=6$, Eq. (4)] and a basis with 171 functions [$i_{\max}=5$, $L_{\max}=5$, Eq. (4)]. The fitting error was assessed using the difference between the two trial fits at 40 000 randomly placed points, and new data point locations were determined using conjugate-gradient optimizations to locate points of maximum squared difference. New points are added in batches of 60 and 60 processors are used to do the 60 *ab initio* calculations. The fitting coefficients were updated (using the dynamic conditioning procedure described above), and the fitting error was estimated. Since the monomers are identical, after each electronic structure calculation, the symmetry partner geometry corresponding to the exchange of the two monomers was also added to the data set. It is noteworthy that no manually located points were included in the fit at any stage. The entire energy and coordinate range was fit without any bias, simply adding points where the automatically estimated error was largest. A specialized IMLS fitting code was developed for this application and can now be conveniently used to automatically generate global PESs for vdW complexes with two rigid fragments.

If an automatically determined geometry is in a region in which the potential is expected to be very large it is rejected. More specifically, we reject points at which a guide surface is more than twice an energy cut-off value that is 15.0 kcal/mol (~ 5246 cm⁻¹) above the dissociation asymptote. For (NNO)₂ the guide surface was constructed using 1600 MP2/2ZaP points chosen from an exponential probability distribution that produces about 17 times as many points with r_0 equal to the shortest value than with r_0 equal to the largest value. A small basis of 40 functions [$i=3$, $L_{\max}=3$, Eq. (4)] was employed (at each data point using IMLS) to construct the guide surface using the MP2/2ZaP data. The guide surface took less than 30 min to construct.

Using the methods outlined in this section we constructed two surfaces (see Sec. IV). The CCSD(T)/3ZaP surface was built from 1646 symmetry unique data points and

has an estimated fitting error below 2 cm^{-1} . The CCSD(T)-F12b/VTZ-F12 surface was terminated at 1757 points with an estimated fitting error below 1.5 cm^{-1} .

III. ELECTRONIC STRUCTURE THEORY

In this section we compare different *ab initio* methods and describe how we chose the two methods used to fit the PESs. The monomers were held rigid at the calculated³³ ground vibrational state averaged bond distances of $R_{\text{NN}} = 1.12872 \text{ \AA}$ and $R_{\text{NO}} = 1.18792 \text{ \AA}$. The size-consistent coupled-cluster CCSD(T) method^{34–37} was chosen to represent the vdW interaction between the two closed-shell NNO monomers. The MOLPRO electronic structure code³⁸ was used for all of the calculations reported here. To confirm the applicability of a single-reference method, the T_1 -diagnostic³⁹ was evaluated at various geometries including points up to $\sim 10\,000 \text{ cm}^{-1}$ above the energy of the separated monomers. For all of the geometries and basis sets tested the T_1 -diagnostic values were ~ 0.02 , indicating that the CCSD(T) single reference method is appropriate for this system.

The complete basis set (CBS) limit was estimated using three different schemes. The first was Peterson's three parameter mixed Gaussian and exponential formula,⁴⁰

$$E(n) = E_{\text{CBS}} + b \exp[-(n-1)+]c \exp[-(n-1)^2]. \quad (7)$$

The second was a Schwenke-style CBS extrapolation,⁴¹

$$E_{\text{CBS}} = [E(n) - E(n-1)]F + E(n-1), \quad (8)$$

where F is a coefficient used to extrapolate total energies and n is the cardinal number of the basis. A third strategy involving separate extrapolation of different components of the total energy was also tested using an optimized power-law, where ℓ_{max} is the cardinal number of the basis and "pow" is an optimized exponent,⁴²

$$E_{\ell_{\text{max}}}^{\text{corr}} = E_{\text{CBS}}^{\text{corr}} + A\ell_{\text{max}}^{-\text{pow}}. \quad (9)$$

Choice of electronic structure methods and bases for (NNO)₂

First we present the results obtained from the methods that are not explicitly correlated. By comparing different bases with and without CP-correction and with and without CBS extrapolation, we determine that a good PES for NNO dimer can be obtained using the 3ZaP basis without a CP-correction and without CBS extrapolation. We denote this surface the exploratory surface. Initial basis set comparisons are done at a set of test points and then at stationary points on the IMLS surface fit to 1646 symmetry unique CCSD(T)/3ZaP points.

The first set of comparisons is done at five high-symmetry test geometries: (1) infinitely separated monomers, (2) a linear head-to-tail geometry with a center of mass separation (r_0) of 6.0 \AA , (3) an attractive parallel side-by-side C_{2v} geometry with $r_0 = 5.0 \text{ \AA}$, (4) a repulsive parallel side-by-side C_{2v} geometry with $r_0 = 3.0 \text{ \AA}$, and (5) the nonpolar minimum, which has C_{2h} symmetry. Energies were com-

TABLE I. Geometric parameters for isomers of NNO dimer located on IMLS fitted PES (CCSD(T)/3ZaP). Distances are in angstroms and angles are in degrees.

Coordinate ^a	Nonpolar O-in	T-shape O-in	Polar	T-shape N-in
r_0	3.443 06	3.888 64	3.649 07	4.196 96
θ_1	60.494	32.100	53.198	78.963
θ_2	119.506	80.005	64.030	19.819
φ_2	180.000	0.000	0.000	0.000
X	0.000	66.048	84.584	119.572

^aSee Fig. 1.

puted at these five points for zeta levels 2–5 of both the Dunning¹⁶ aug-cc-pVnZ (AVnZ) and the Petersson⁴³ nZaP (with $n=2, 3, 4$, and 5) bases. At all five points, the nZaP and AVnZ bases extrapolated to about the same CBS energies [using total energies with Eq. (7) and $n=3, 4$, and 5]. These are considered as benchmark values for the calculations that are not explicitly correlated. However, for the purpose of computing a surface, we exclude the Eq. (7) extrapolation and the AVnZ bases. Equation (7) is not used because it requires energies from at least three zeta levels, and quadruple and higher zeta were deemed too expensive. The 2ZaP and 3ZaP bases were less costly respectively than the AVDZ and AVTZ bases and so, for making the PES, we therefore opt for the Petersson bases. Equation (8) was tested using 2ZaP and 3ZaP energies with and without CP-corrections. The parameter F [in Eq. (8)] was fit to the CBS energies previously determined using Eq. (7). The value of F determined by Eq. (8) differed at each test point. Choosing F as the average from test points 3–5 caused problems. Equation (8) has the advantage that it does not require bases larger than triple zeta, but it is known that including double zeta energies in a CBS extrapolation may introduce significant error⁴¹ and we therefore anticipated the possibility of problems with the CBS extrapolation. Extrapolation of energies without CP-corrections produced a well depth of only $\sim 450 \text{ cm}^{-1}$, whereas the CBS benchmark obtained using Eq. (7) and zeta levels 3–5 was $\sim 600 \text{ cm}^{-1}$. The large effect of basis set superposition error (BSSE) on the double zeta energies also resulted in a small nonphysical barrier for extrapolated energies at large separations (e.g., test point 2). The use of CP corrected energies eliminated the nonphysical barrier, and better represented the well depth, but produced energies that were far too attractive on the repulsive wall (e.g., test point 4). Without the CP-correction, the raw 3ZaP energies are in surprisingly good agreement with the benchmark CBS energies, more accurate than 3ZaP+CP, or any 2–3 CBS extrapolation, at all five test points. The CCSD(T)/3ZaP method, without CP-correction and without CBS extrapolation, was therefore chosen for fitting the exploratory surface.

Further tests were done at the minima of the exploratory surface. Results are given in Tables I and II and Fig. 2. Geometric parameters for various isomers are listed in Table I. Without CP-corrections, starting from too low at the double zeta basis, convergence was oscillatory for all of the minima. With CP-corrections, convergence was monotonic at each structure, but the minima were much too shallow for the

TABLE II. *Ab initio* energies for isomers on the 3ZaP PES (see Fig. 2).

Theory ^a	Nonpolar O-in	T-shape O-in	Polar	T-shape N-in
2ZaP	-939.85	-743.16	-684.22	-675.27
3ZaP	-601.53	-438.07	-445.83	-444.02
4ZaP	-579.40	-393.47	-422.00	-397.96
5ZaP	-599.35	-395.01	-433.10	-398.24
CBS	-611.29	-396.12	-439.78	-398.61
2ZaP+CP	-356.26	-227.05	-216.20	-250.35
3ZaP+CP	-405.06	-264.55	-278.40	-290.60
4ZaP+CP	-504.81	-326.58	-358.80	-343.46
5ZaP+CP	-561.27	-363.29	-400.79	-371.11
CBS	-594.34	-384.80	-425.36	-387.29
IMLS ^b	-602.32	-440.91	-444.38	-442.36
Fitting error	-0.79	-2.84	1.45	1.66

^aCCSD(T)/*n*ZaP energies (cm^{-1} , relative to separate monomers), +CP indicates counterpoise correction, CBS evaluated using zeta levels 3–5 and Eq. (7).

^bIMLS surface fit to 3ZaP data.

smaller bases. Furthermore, with CP-corrections, in most cases the energy decreased more between zeta levels 3 and 4 than between levels 2 and 3. The CBS energies from the basis series with and without CP-corrections are quite similar for each structure, generally agreeing to within 10 and 15 cm^{-1} . For two of the minima, the non-CP corrected 3ZaP results are remarkably close to the benchmark CBS values. The global minimum (nonpolar O-in) and polar minimum are both within 10 cm^{-1} of the CBS energies. Energies at the stationary points on the fitted surface are plotted as a function of disrotatory coordinate X [Eq. (3)] connecting the four minima and four transition structures (TSs) in Figs. 3(a) and 3(b). These results at the minima confirm the 3ZaP, no CP, no CBS choice made on the basis of results at the high-symmetry test points.

Although the larger Dunning basis sets are too expensive for the purpose of making a PES, it may be of interest to compare energies computed with them. Results with the Dunning AV*n*Z basis series for the same stationary point structures are shown in Fig. 4. For reference, Fig. 4 includes benchmark CBS energies from explicitly correlated F12b calculations described in the next paragraph. Without CP-corrections, energies change little between AVDZ and AVTZ and the agreement with the CBS energies worsens at several points; but from AVTZ to AVQZ the improvement is significant. With CP-corrections the wells are much too shallow at the double zeta level, but improve monotonically with zeta level, with the AVQZ+CP results quite close to the CBS limit. These results are quite different than those obtained using the *n*ZaP bases. Without CP-corrections the 4ZaP energies are close to CBS values, whereas the AVQZ energies

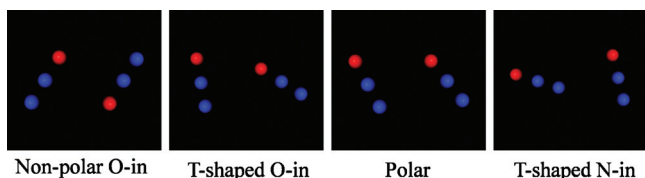


FIG. 2. Structures corresponding to minima on 3ZaP PES (see text and Tables I and II).

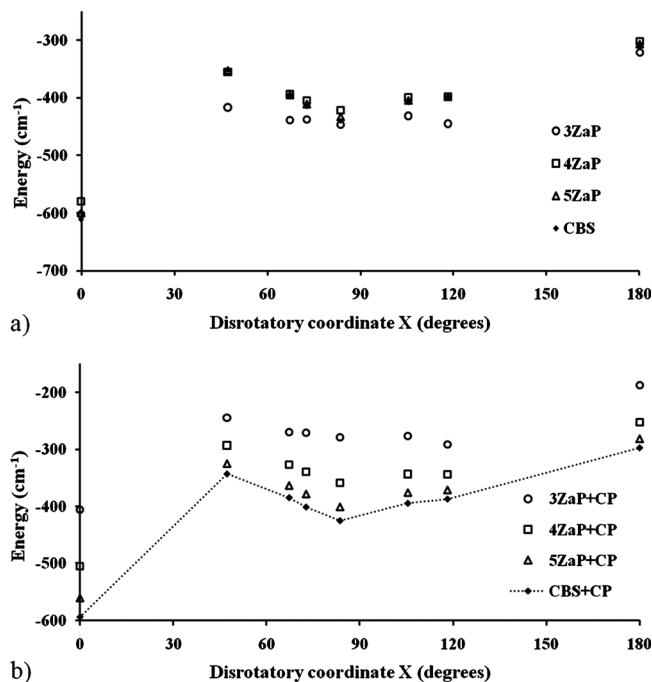


FIG. 3. CCSD(T) energies of eight stationary points on the 3ZaP IMLS surface calculated with (a) larger bases and (b) larger bases with CP-corrections.

are still quite far from convergence. Conversely, with CP-corrections the AVQZ+CP energies are very close to CBS values, whereas the 4ZaP+CP energies are far from convergence.

The 3ZaP PES is certainly qualitatively correct but there is reason to believe that even better *ab initio* calculations would give us a superior surface. The most significant failing of the 3ZaP basis is its prediction that T-shape N-in and T-shape O-in structures have energies close to that of the polar minimum. Energies at these T-shape points are roughly 40–55 cm^{-1} higher in the CBS limit. We therefore applied explicitly correlated F12b methods⁴⁴ to NNO dimer. In the rest of this section we explain how the basis to be used with the F12b method is chosen and whether to use a CBS extrapolation.

Single-point CCSD(T)-F12b energies were calculated using the AV*n*Z bases with $n=2-5$ (the largest calculation taking about one week) and the Peterson V_nZ -F12 bases

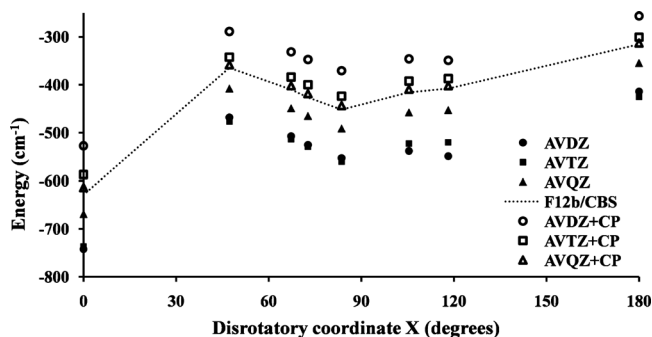


FIG. 4. Energies of eight stationary points on the 3ZaP IMLS surface: AVDZ, AVTZ, and AVQZ results with and without CP-correction are presented for the standard CCSD(T) method (CCSD(T)-F12b/CBS energies are shown for comparison).

TABLE III. Explicitly correlated CCSD(T)-F12b calculations of well depth.

Theory ^a	Reference	CCSD-F12b	(T)	Total	Well depth ^b
Monomer					
AVTZ	-183.761 329 66	-0.677 001 70	-0.036 108 58	-184.474 439 94	
AVQZ	-183.765 109 45	-0.683 916 62	-0.038 691 78	-184.487 717 85	
AV5Z	-183.765 668 64	-0.685 661 50	-0.039 661 71	-184.490 991 85	
CBS	-183.765 985 00	-0.686 745 30	-0.040 779 97	-184.493 510 28	
Dimer					
AVTZ	-367.523 616 79	-1.355 894 14	-0.072 445 87	-368.951 956 80	-675.31
AVQZ	-367.531 100 09	-1.369 676 45	-0.077 612 55	-368.978 389 08	-648.19
AV5Z	-367.532 208 61	-1.373 136 36	-0.079 550 37	-368.984 895 34	-639.03
CBS	-367.532 835 81	-1.375 270 50	-0.081 779 97	-368.989 886 29	-628.96

^aCCSD(T)-F12b/*AVnZ* energies (a.u.) calculated using size consistent F12b 3C(FIX) ansatz, CBS evaluated using zeta levels 3–5 and Eq. (7).

^bWell depth calculated using dimer and monomer energies at each zeta level (units of cm^{-1}).

with $n=2-3$.⁴⁵ Values for the geminal Slater exponent β were chosen for each basis as recommended by Hill.⁴² To determine the CBS limit at the global minimum for this method, the reference energies were extrapolated using Eq. (7), while the CCSD-F12b and (T) components of the correlation energy were separately extrapolated using the optimized power-law of Eq. (9), where ℓ_{\max} is the cardinal number of the basis and pow is an optimized exponent.

Table III shows the results of the explicitly correlated calculations at the 3ZaP global minimum geometry for each zeta level of the *AVnZ* basis sets. The well depth calculated using the explicitly correlated F12b method converges monotonically to -628.96 cm^{-1} , slightly lower than either progression in Table II. The F12b energies converge rapidly with zeta level, changing only in small steps beyond the triple zeta level in contrast to the CP-corrected conventional CCSD(T) method which also converged monotonically, but where the energy changed by $\sim 56 \text{ cm}^{-1}$ between quadruple and quintuple zeta. The rapid convergence behavior of the F12b energies results in robust CBS extrapolation. Simply extrapolating the AVTZ and AVQZ CCSD(T)-F12b total energies using a nonoptimized $\text{pow}=3$ [in Eq. (9)] produces a CBS well depth of -628.41 (within 0.6 cm^{-1} of the result obtained above including AV5Z energies and optimized separate extrapolation of different components of the total energy). In Table IV and Fig. 5, CCSD(T)-F12b energies are

plotted at the eight stationary points of the 3ZaP-IMLS surface (cf. Figs. 3 and 4).

Given the rapid convergence of the F12b method, the other CBS energies in Table IV were estimated using AVTZ and AVQZ energies and $\text{pow}=3$ [in Eq. (9)]. The relative energies of isomers from even the double zeta basis calculations agree qualitatively with those of the CBS extrapolation. The performance of the Peterson *VnZ*-F12 bases is particularly impressive. As shown in Table IV and Fig. 5(b), the basis set error at these eight points is very small even at the double zeta VDZ-F12 level, where mean and rms errors relative to CBS are 8.70 and 10.59 cm^{-1} , respectively. For comparison the mean and rms basis set errors with the AVQZ basis and the F12b method are 17.70 and 17.72 cm^{-1} . The mean and rms errors with the VTZ-F12 basis are very small, 1.92 and 2.61 cm^{-1} (well within the uncertainty of the CBS extrapolations). Due to the high-accuracy of the *VnZ*-F12 basis results, only the errors are plotted in Fig. 5(b). The *VnZ*-F12 bases are larger at each zeta level than either the *nZaP* or *AVnZ* bases making them more costly to use. The numbers of contracted functions for $(\text{NNO})_2$ are 180 (VDZ-F12) and 318 (VTZ-F12), compared to 108 (2ZaP), 204 (3ZaP), 138 (AVDZ), and 276 (AVTZ). Given the remarkable performance of the explicitly correlated F12b method and the VTZ-F12 basis in particular, the CCSD(T)-

TABLE IV. Explicitly correlated CCSD(T)-F12b calculations for isomeric minima and TSs located along disrotatory coordinate *X* on the fitted 3ZaP/IMLS PES.

Theory ^a	Non-polar O-in	TS1	T-shaped O-in	TS2	Polar	TS3	T-shaped N-in	TS4
VDZ	-960.04	-538.85	-660.86	-692.81	-732.42	-642.54	-635.13	-527.46
AVDZ	-801.22	-512.18	-536.25	-548.72	-584.19	-524.04	-502.12	-412.97
VTZ	-706.21	-407.26	-470.55	-490.56	-520.40	-474.66	-463.40	-376.32
AVTZ	-675.31	-406.04	-449.08	-466.63	-495.05	-458.10	-450.56	-362.04
AVQZ	-648.19	-382.05	-426.38	-443.35	-469.94	-433.63	-425.88	-336.98
AV5Z	-639.03							
CBS	-628.96	-364.54	-409.82	-426.35	-451.63	-415.77	-407.88	-318.69
VDZ-F12 ^b	-605.73	-359.65	-398.90	-415.49	-442.05	-409.28	-408.02	-309.31
VTZ-F12 ^b	-625.09	-363.34	-409.64	-427.05	-452.66	-416.53	-408.24	-320.27

^aCCSD(T)-F12b energies (cm^{-1}) relative to separate monomers at each basis set level. CBS schemes are discussed in the text.

^bRefers to bases optimized for the F12 method (Ref. 43).

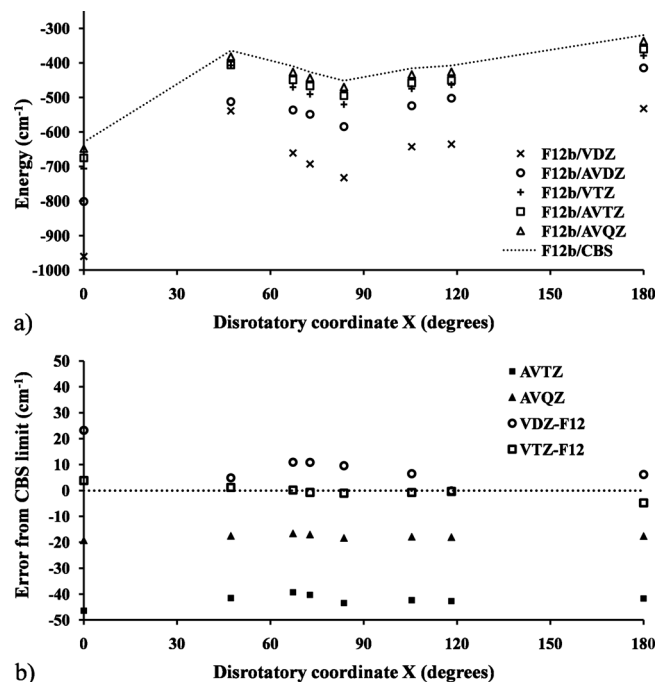


FIG. 5. Energies of eight stationary points on the 3ZaP IMLS surface: (a) CCSD(T)-F12b energies are compared for VDZ, AVDZ, VTZ, AVTZ, AVQZ, and CBS (see text). (b) Basis set errors for AVnZ and VnZ-F12 bases.

F12b/VTZ-F12 method (without additional CBS extrapolation) was selected to construct a high-accuracy global PES for use in dynamics studies.

IV. APPLICATION OF THE FITTING METHOD TO (NNO)₂

The IMLS automatic surface generator was run in parallel with 60 processes. The coordinate range includes all attractive energies and repulsive energies up to 15.0 kcal/mol (~ 5246 cm⁻¹) above the separate monomers asymptote. The CCSD(T)/3ZaP surface was terminated with 1646 symmetry unique data points when the estimated fitting error was below 2 cm⁻¹. The CCSD(T)-F12b/VTZ-F12 surface was terminated with 1757 points with an estimated fitting error below 1.5 cm⁻¹. These estimated fitting errors are obtained from differences between two surfaces for which the local fits are done with different fitting basis sets. In previous work it has been demonstrated that these estimated fitting errors provide a reliable measure of the true fitting error.²³ To confirm that this is also the case for NNO dimer (given the particular coordinates and fitting basis set) we did extensive testing using a low-level *ab initio* method (MP2/2ZaP). In several test fits, at each iteration (after each set of 60 new *ab initio* data was added to the PES), the error estimated using the difference between two fits at 40 000 randomly selected points was compared with the *real* error computed using new *ab initio* data at 600 randomly chosen test points. In this way the estimated fitting error was shown to be reliable for the current application of IMLS.

The 3ZaP potential is qualitatively similar to the F12b surface but has additional stable minima corresponding to T-shaped O-in structures. Geometries of four symmetry

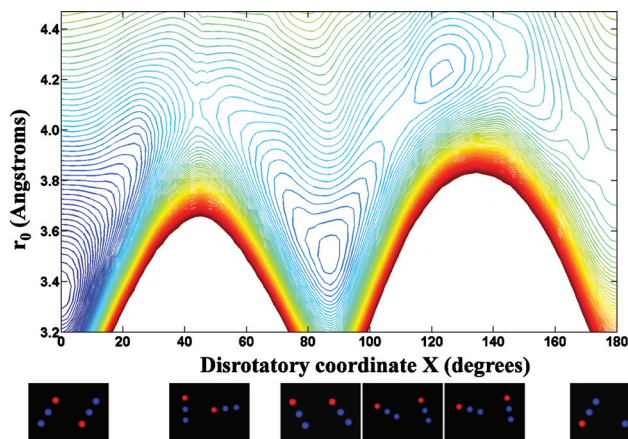


FIG. 6. Contour plot of F12b PES r_0 and disrotatory coordinate X [with minimization of conrotatory coordinate Y, see text and Eq. (3)]. Structures corresponding to six stationary points are shown at the bottom.

unique minima (all planar) are shown in Table I and Fig. 2. Experimentally, only the nonpolar O-in and the polar structure have been observed.

The F12b PES has two polar minima, two T-shaped N-in minima, and a global nonpolar minimum (shown in Fig. 6) connected by transition structures, but has no minima at T-shaped O-in structures. The second polar and T-shaped isomers are related to their respective partners by symmetry and would appear between -180° and 0° along the disrotatory coordinate in Fig. 6 (not shown). Essential features of the dynamics of NNO dimer can be understood in terms of the disrotatory coordinate X that connects the planar minima and transition structures.

Starting at $X=0$ (nonpolar O-in global minimum at the left of Fig. 6), the monomers are set antiparallel with $\theta_1 + \theta_2 = 180^\circ$. As X is increased, monomer 1 on the left rotates counterclockwise, while monomer 2 on the right rotates clockwise. When X reaches 180° , each monomer has flipped around 180° (nonpolar N-in TS at the right of Fig. 6). Along the disrotatory coordinate the potential is symmetric about $X=0$. To make the plot in Fig. 6, φ is set equal to zero or π (system is planar) and the energy, for given values of r_0 and X, is minimized with respect to the conrotatory coordinate Y. Since all of the minima and TSs are planar (no out of plane TSs were located), all of the critical points and minimum energy paths connecting them are shown in Fig. 6. The TS structures were optimized using a Newton-Raphson algorithm on the fitted surface. The energies and structural parameters for the six critical points located on the F12b PES (shown in Fig. 6) are given in Table V.

The barrier to isomerization between the polar and nonpolar O-in isomers is ~ 95 cm⁻¹ (from the polar isomer side). The barrier between the T-shaped N-in and polar isomers is only ~ 15 cm⁻¹ (from the T-shaped isomer). Rotational constants calculated (experimental values in parentheses) by simply using the minimum energy structures are $A = 0.299\ 93(0.299\ 41)$, $B = 0.061\ 88(0.059\ 93)$, and $C = 0.051\ 300(0.049\ 84)$ cm⁻¹ and are in fairly good agreement with experiment. In Sec. V we report rovibrational calcula-

TABLE V. Energies and geometric parameters for isomers of N₂O dimer located on IMLS fitted PES (CCSD(T)-F12b/VTZ-F12).

Coordinate ^a	Nonpolar O-in	TS1	Polar	TS2	T-shaped N-in	TS3
r_0	3.359 16	4.102 21	3.499 00	4.052 28	4.231 59	3.805 48
θ_1	61.171	91.648	57.774	71.447	80.909	123.072
θ_2	118.829	173.862	63.904	30.105	14.815	56.928
φ_2	180.000	180.000	0.000	0.000	0.000	180.000
X	0.000	42.755	86.935	110.671	123.047	180.000
Energy ^b	-633.43	-360.21	-465.20	-406.76	-421.03	-322.85

^aSee Fig. 1.^bEnergies relative to separate monomers.

tions using the F12b PES, which, due to the inclusion of anharmonicity and coupling, produce rotational constants in much better agreement with experiment.

V. ROVIBRATIONAL CALCULATIONS

A. Methods

Polyspherical coordinates are used to compute the energy levels.^{46,47} The monomers are rigid and the intermolecular coordinates are defined using three vectors: \mathbf{r}_1 , \mathbf{r}_2 , and \mathbf{r}_0 . Vector \mathbf{r}_1 is aligned with NNO monomer 1 and points toward O. Vector \mathbf{r}_2 is similarly defined for monomer 2. Vector \mathbf{r}_0 points from the center of mass of monomer 1 to that of monomer 2 (as shown in Fig. 1). There are four vibrational coordinates: θ_1 (θ_2), the angle between \mathbf{r}_0 and \mathbf{r}_1 (\mathbf{r}_2); φ_2 , a dihedral angle from \mathbf{r}_1 to \mathbf{r}_2 around \mathbf{r}_0 ; and r_0 , the length of \mathbf{r}_0 . Euler angles specify the orientation of a body-fixed frame attached such that the z axis is along \mathbf{r}_0 and the x axis is along the vector $\mathbf{r}_0 \times \mathbf{r}_1 \times \mathbf{r}_0$. The kinetic energy operator in these coordinates is well known.^{46,48–50}

For the stretch coordinates we use discrete variable representation (DVR) functions,^{51–54} and for the bend and rotational coordinates we use parity adapted rovibrational functions^{55,56} ($\bar{m}_2 = -m_2$ and $\bar{K} = -K$),

$$|u_{l_1 l_2 m_2; K}^{JMP}\rangle = N_{m_2, K} \frac{1}{\sqrt{2}} [|l_1 l_2 m_2; JKM\rangle + (-1)^{J+P} |l_1 l_2 \bar{m}_2; J\bar{K}\bar{M}\rangle], \quad (10)$$

with $N_{m_2, K} = (1 + \delta_{m_2, 0} \delta_{K, 0})^{-1/2}$. The ket in this equation is defined by

$$\begin{aligned} & \langle \theta_1, \theta_2, \varphi_2; \alpha, \beta, \gamma | l_1 l_2 m_2; JKM \rangle \\ &= \sqrt{\frac{2J+1}{8\pi^2}} \Theta_{l_1}^{m_1}(\theta_1) Y_{l_2}^{m_2}(\theta_2, \varphi_2) D_{MK}^J(\alpha, \beta, \gamma)^*, \end{aligned} \quad (11)$$

with

$$Y_{l_2}^{m_2}(\theta_2, \varphi_2) = \frac{1}{\sqrt{2\pi}} \Theta_{l_2}^{m_2}(\theta_2) e^{im_2\varphi_2}, \quad (12)$$

$$m_1 \equiv K - m_2,$$

where $\Theta_l^m(\theta)$ is a normalized associated Legendre function with the $(-1)^m$ Condon–Shortley phase factor. D_{MK}^J is a Wigner function⁵⁷ and (α, β, γ) are the Euler angles. For the parity adapted functions, $K \geq 0$ and $P=0$ and 1 correspond to

even and odd parities. If $K=0$ it is necessary to apply the constraint $m_2 \geq 0$. The combination $m_2=K=0$ and $(-1)^{J+P} = -1$ is not allowed. In our calculations l_1 , l_2 , and m_2 all have the same maximum value. The parity adapted basis makes it possible to calculate even and odd parity levels separately. The $J=0$ even-parity angular functions are also used, as explained in Sec. II, to construct the potential energy surface. They can be explicitly written as

$$|u_{l_1 l_2 m_2; K=0}^{J=0, M=0, P=0}\rangle = \frac{1}{\sqrt{(1 + \delta_{m_2, 0})\pi}} \Theta_{l_1}^{-m_2}(\theta_1) \Theta_{l_2}^{m_2}(\theta_2) \cos(m_2\varphi_2). \quad (13)$$

A complete product basis function is $f_{\alpha_0}(r_0) u_{l_1 l_2 m_2; K}^{JMP}(\theta_1, \theta_2, \varphi_2; \alpha, \beta, \gamma)$, where $f_{\alpha_0}(r_0)$ is a potential-optimized DVR (PODVR) function.^{58,59}

We use a symmetry adapted variant^{60,61} of the Cullum and Willoughby⁶² Lanczos method to compute the energy levels. This makes it possible to do a single calculation for each parity block that yields both the symmetric and anti-symmetric states with respect to permuting the two NNO monomers. To use the Lanczos algorithm to compute energy levels, it is not necessary to store the Hamiltonian matrix representing the Hamiltonian in the complete multidimensional basis. Instead, one must store only a few vectors. Eigenvalues are obtained by computing matrix-vector products. Similar techniques have been used to compute energy levels of many molecules.^{52,63} The full permutation-inversion (PI) symmetry group for the Hamiltonian we use is G_4 , composed of operations $\{E, \sigma_{ex}\} \otimes \{E, E^*\}$, where σ_{ex} permutes monomer 1 with monomer 2. A/B label symmetric and antisymmetric irreducible representations (irreps) with respect to σ_{ex} and $+/-$ label even and odd parities. There are four PI irreps: A+, B+, A-, and B-. To use the symmetry adapted Lanczos algorithm within each parity block to obtain A and B states, one must make projection operators for these irreps. To do this one must determine how the symmetry operations affect the coordinates.⁶⁴ The effect of the symmetry operations on the rovibrational coordinates and basis functions is given in Table IV of Ref. 64. For example,

$$\begin{aligned} & \sigma_{ex}(\theta_1, \theta_2, \varphi_2, \alpha, \beta, \gamma) \\ & \rightarrow (\pi - \theta_2, \pi - \theta_1, \varphi_2, \pi + \alpha, \pi - \beta, -\gamma - \varphi_2). \end{aligned} \quad (14)$$

Matrix-vector products are evaluated by doing sums sequentially.^{47,52,65,66} Similar techniques have been used to compute energy levels of many molecules.^{52,63,67–69} Kinetic

energy matrix-elements are in Ref. 70. Potential matrix-vector products are evaluated by using quadrature and doing sums sequentially, as explained in Ref. 70. The wave functions are obtained from eigenvectors of the Hamiltonian matrix that are computed as described previously.^{55,71} At the global potential minimum, (NNO)₂ has a slipped antiparallel structure with C_{2h} point group symmetry. The PI irreps A+, B+, A−, and B− correlate with A_g, B_u, A_u, and B_g of the C_{2h} group, respectively. There are four intermolecular vibrational modes whose quantum numbers are denoted by (in the order of increasing energy) v_t (A−, torsion), v_g (B+, geared bend), v_r (A+, vdW-stretch), and v_a (A+, antigeared bend). Geared and antigeared coordinates are defined in terms of the polyspherical angles by $\rho_g = \theta_1 + \theta_2$ (B+) and $\rho_a = \theta_1 - \theta_2$ (A+). The A/B symmetry assignment is due to Eq. (14).

B. Results

The monomer rotational constant is taken to be the experimental ground state value of 0.419 011 cm^{−1}.⁷² The masses are 14.003 074 005 2 and 15.994 914 622 1 amu for N and O, respectively. For the angular basis we use $l_{\max} = m_{\max} = 44$ (the same l_{\max} for l_1 and l_2). We use 45 Gauss–Legendre quadrature points for θ_1 and θ_2 , and 90 equally spaced trapezoid points in the range $[0, 2\pi]$ for φ_2 , with the first point zero. For r_0 we use 25 PODVR functions.^{58,59} The reference potential that defines the PODVR functions is a cut potential defined in the range (4.5 bohr, 18.0 bohr). Tests confirm that this basis set converges levels near 100 cm^{−1} above the zero point energy (ZPE) to better than 0.001 cm^{−1}. The vibrational even-parity basis size is about 628 000, built from 31 395 even-parity angular basis functions. We use a potential ceiling to reduce the spectral range.⁶³ About 82% of the quadrature points are below the ceiling value of 5240 cm^{−1}.

Although the F12b PES is global, and we have obtained results for the polar and T-shaped N-in isomers, in this paper we concentrate on vibrational states in the nonpolar O-in well. A detailed treatment of rovibrational states corresponding to the other isomers and mixed isotopomers, including tunneling splittings, will be the subject of a forthcoming publication.

A good description of the dynamics of NNO dimer could be obtained by exploiting the difference between the intramonomer stretches and the intermonomer coordinates. To do this one would average the full potential over products of monomer wave functions to obtain effective intermonomer potentials. There would be one such potential for each product of monomer states. These potentials would then be used with different rotational constants for different products of monomer states to compute intermolecular levels. We cannot implement this strategy because the potential we have constructed is 4D and depends only on the intermolecular coordinates. The 4D potential we have fit fixes the remaining coordinates at their calculated monomer ground vibrational state averaged values. For all our calculations we use the ground state monomer rotational constant given above.

Vibrational levels of (NNO)₂ in the nonpolar O-in global minimum are listed in Table VI. Most of the levels are as-

TABLE VI. The lowest vibrational levels (in cm^{−1}) of (NNO)₂ for each irrep relative to the ZPE of −514.2118 cm^{−1}. The quantum numbers v_t (torsion), v_g (geared bend), v_r (vdW-stretch), and v_a (antigeared bend) are for the four intermolecular modes.

A+	B+	A−	B−
0.0000(0000)	41.8609(0100)	25.7599(1000)	65.6419(1100)
50.7624(2000)	86.7299(0110)	74.5621(3000)	109.9291(1110)
52.7591(0010)	90.3303(2100)	77.2499(1010)	113.9184(3100)
80.4367(0200)	114.1504(0300)	104.0559(1200)	138.5431
97.5221(0001)	128.4750	121.2341(5000)	151.6697
98.1581(4000)	132.7743(2110)	121.5410(1001)	154.5332
101.0072(2010)	135.4885(0101)	124.1867(3010)	157.6977
101.9135(0020)	137.2096(4100)	125.2602(1020)	159.6448
116.5749(0210)	143.5294(polar)	141.0917(1210)	
127.9299(2200)	143.8152(0310)	150.2890(3200)	
140.2778(0011)		164.1595	
143.5294(polar)		164.8119(7000)	
143.7790(6000)			
144.2993(4001)			

signed (v_t, v_g, v_r, v_a) quantum numbers. The ground state of the polar isomer appears as a pair of degenerate levels (A+, B+) at 143.5294 cm^{−1}. The dynamics of the polar and T-shaped N-in isomers will be discussed in a forthcoming publication.

Examining probability density (PD) plots is essential for assigning vibrational levels. We have computed one-dimensional (1D) and two-dimensional PDs by integrating over the other three or two (respectively) coordinates. PD plots for coordinate pairs (θ_1, θ_2) , (θ_2, φ_2) , (θ_2, r_0) , and (φ_2, r_0) are presented in Figs. 7–10. The four 1D plots are not shown. We first discuss the salient features of the $J=0$ intermolecular vibrational states. The simplest wave functions are those associated with torsional states for which a progression up to $v_t=7$ is evident; see Fig. 7.

Clearly coupling between the torsion and other coordinates is weak. The v_t assignments given in Table VI are unambiguous. PDs of geared states are shown in Fig. 8.

The probability density plots for the geared states have a clear nodal structure up to $v_g=3$, above which they are distorted by coupling. States that involve excitation of the vdW-stretch and the antigeared coordinate are not as simple. In fact even their fundamentals show signs of coupling; see Fig. 9.

The $v_r=1$ state has some antigeared character, as shown by the elongation along the $\theta_1 - \theta_2$ direction in the (θ_1, θ_2) PD plot. The fact that the two bumps in the (θ_2, r_0) PD plot are not centered on the same θ_2 values is also a manifestation of the coupling between θ_2 and r_0 . The same coupling also affects the $v_a=1$ state and this is seen in the (θ_2, r_0) PD of the $v_a=1$ state. The vdW-stretch mode couples not only to the antigeared mode, but also to the geared mode, as shown in the PD plots for the (0110) state ($E=86.7$ cm^{−1}, B+), see Fig. 10. The lobes in the (θ_1, θ_2) plot (Fig. 10) have structure in the $\theta_1 - \theta_2$ direction similar to that of the vdW-stretch state. In addition, coupling between the vdW-stretch and the geared mode is responsible for the tilt of the (r_0, θ_2) PD. Couplings between the geared and the vdW-stretch modes

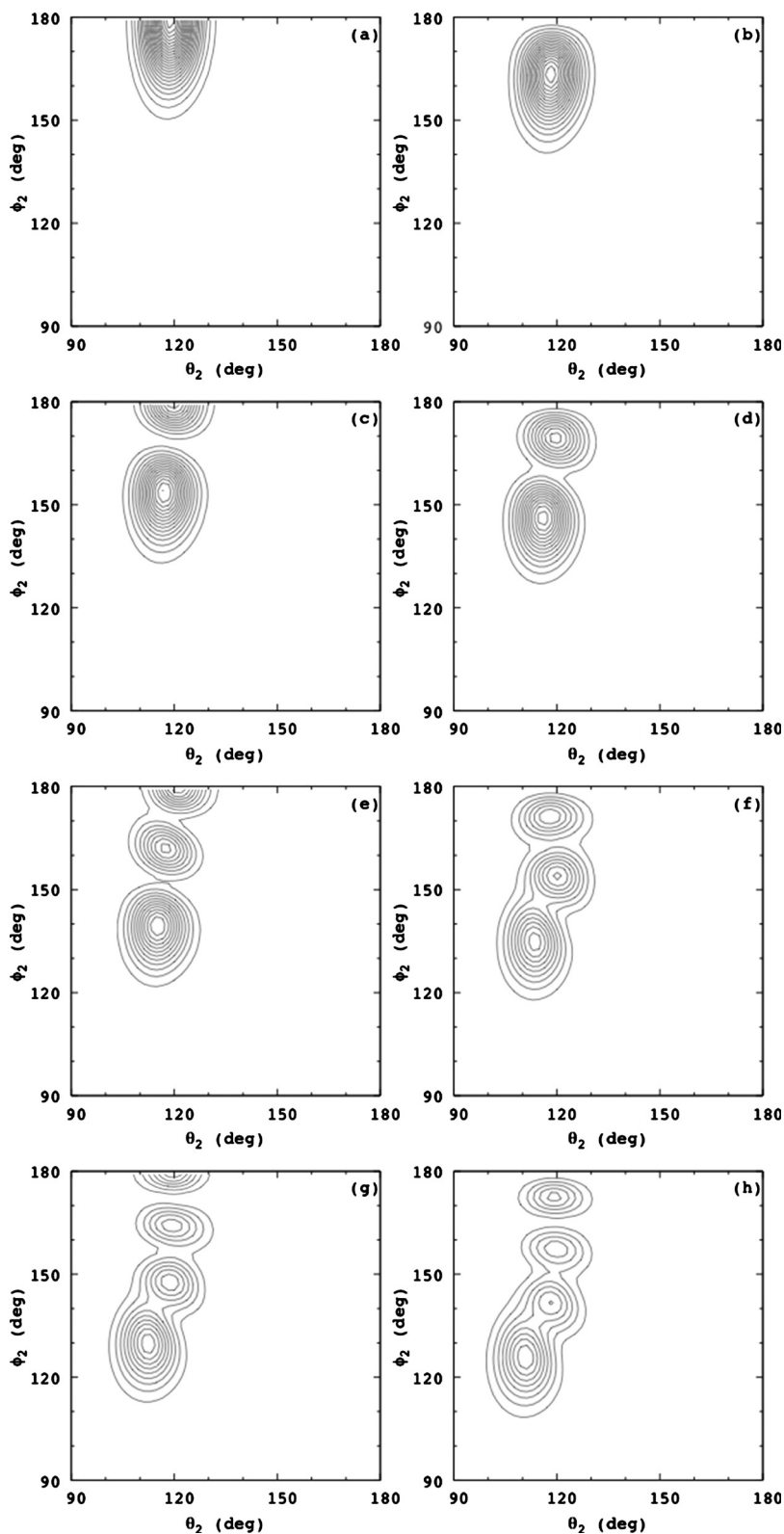


FIG. 7. Probability density plots for torsional states $\nu_1 = 0-7$ [(a)–(h)]. No strong coupling to other modes is observed. The contour interval is 0.4 and the smallest (outermost) contour is 0.4.

and between the antigear and the vdW-stretch modes are found to also influence higher states and hamper assigning these levels.

Moazzen-Ahmadi and co-workers measured IR spectra that probe transitions from the ground state to combination levels near 2200 cm^{-1} involving the in-phase ν_1 vibration, where ν_1 is the antisymmetric stretch NNO monomer mode and in-phase means that the two monomers vibrate in phase.

Using an estimated (hence, the error bar of 1.0 cm^{-1}) band center for the in-phase ν_1 vibration which is not IR active, they find torsion¹² and geared¹³ band centers at $27.3(1.0)$ and $42.3(1.0)\text{ cm}^{-1}$, respectively. These compare well with our results of 25.76 and 41.86 cm^{-1} , respectively, but note that our results are not obtained from combinations. To compute the measured quantity we would need to add two more coordinates (associated with the ν_1 vibration of each monomer)

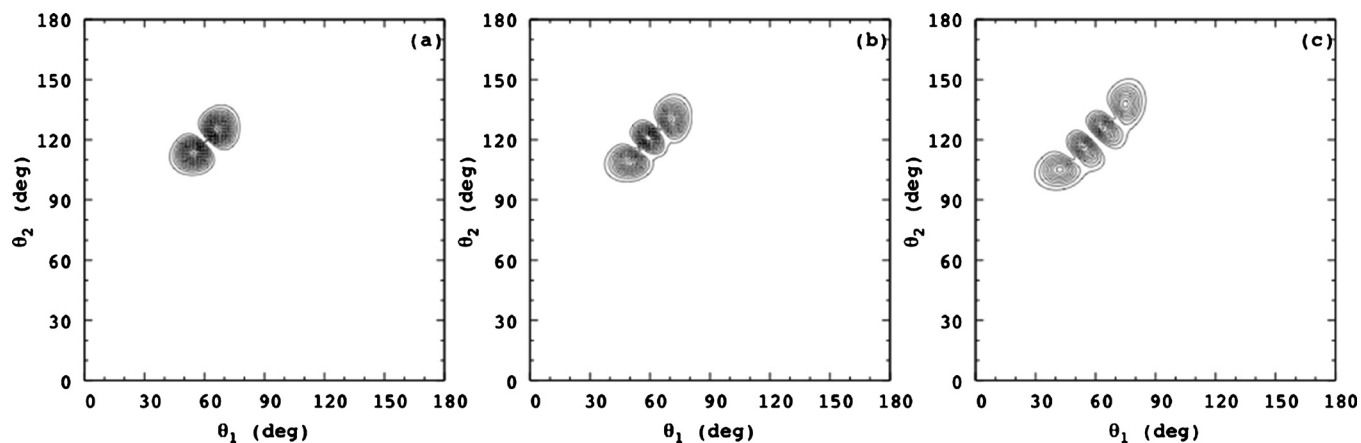


FIG. 8. Probability density plots for the geared states $v_g=1-3$ [(a)–(c)]. Geared states with more quanta ($v_g \geq 4$) show evidence of coupling. The contour interval is 0.5 and the smallest (outermost) contour is 0.5.

to obtain a six-dimensional potential energy surface. As expected, our torsion and geared energies are lower than the CCSD/AVDZ *ab initio* harmonic numbers of 30 and 49 cm^{-1} .¹⁵

Rotational levels are assignable for many vibrational states. Table VII gives assignments for $J=1$ levels. Energy

spacing and a product symmetry rule are used to make the assignment. According to the product symmetry rule the rovibrational level symmetry is a product of the vibrational symmetry and the rotational symmetry. The symmetry of the vibrational levels is known. There are two ways to obtain the symmetry of the rotational wave functions: (1) associate the

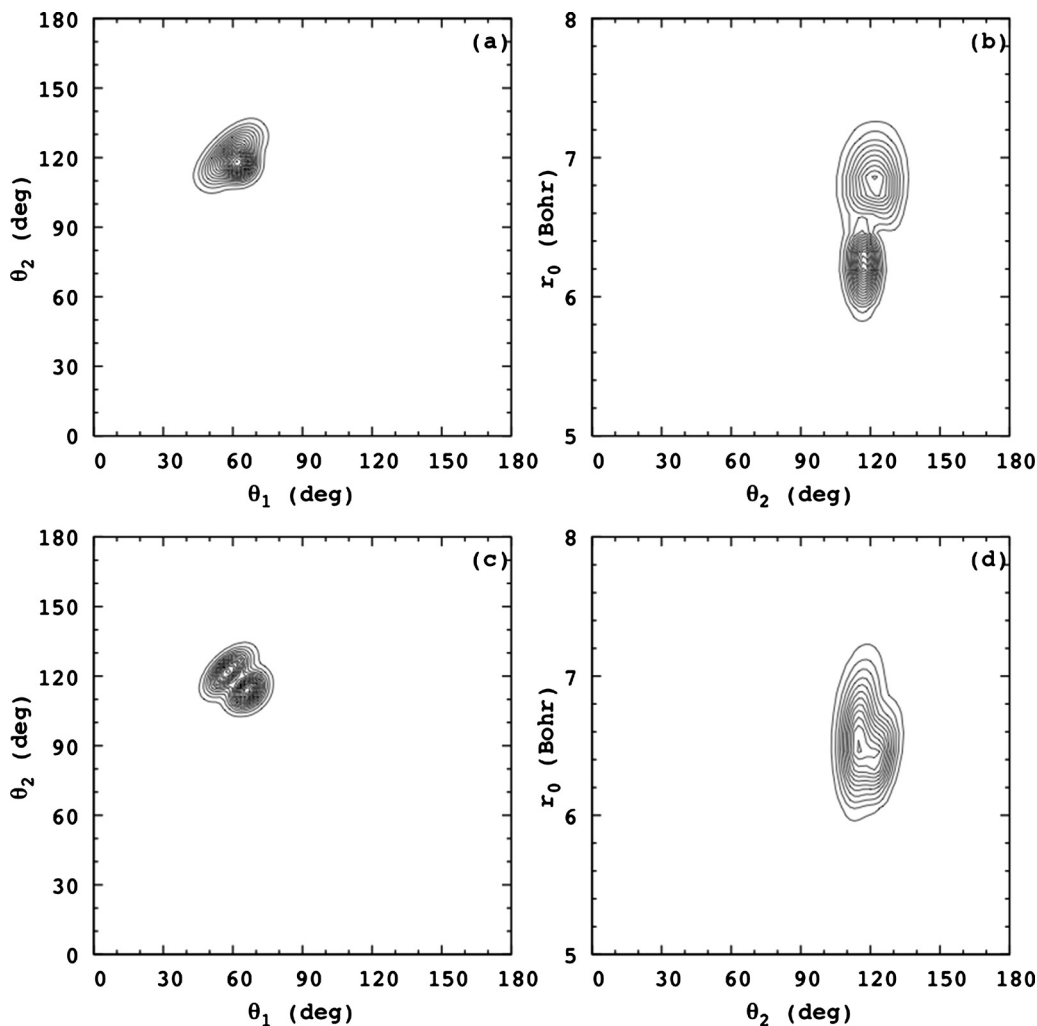


FIG. 9. The vdW-stretch fundamental state ($v_r=1$) (top two panels) and the antigeared fundamental state ($v_a=1$) (bottom two panels) are plotted showing the coupling between the two modes. The contour interval is 0.5 and the smallest (outermost) contour is 0.5.

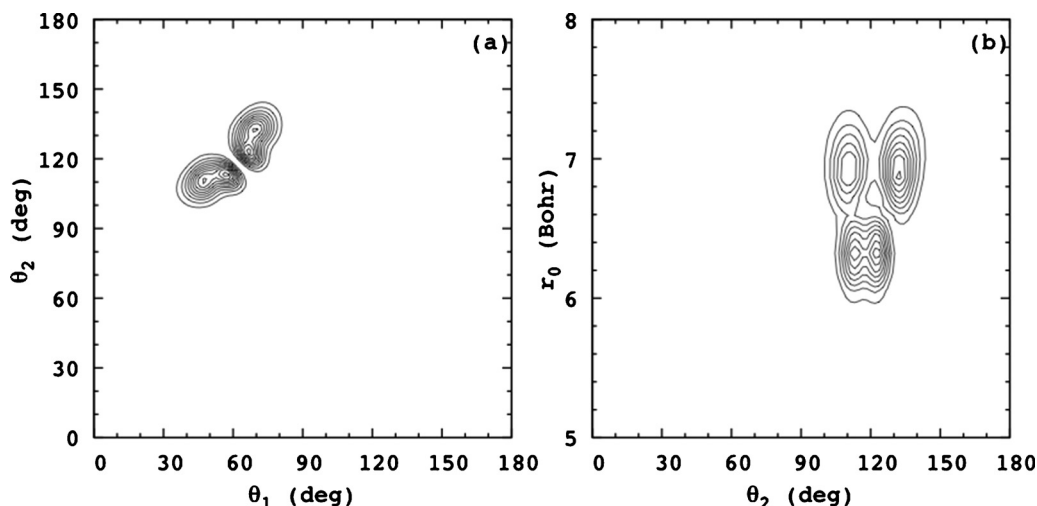


FIG. 10. The vdW-stretch and geared combination state (0110) showing coupling between the two modes. The contour interval is 0.5 and the smallest (outermost) contour is 0.5.

rotational wave functions with rotation of a rigid shape and establish a relationship between the evenness or oddness of K_a , K_c , and irreps using the asymmetric top symmetry rule;⁷³ (2) use assigned $J=1$ levels and their symmetries to establish a relationship between the evenness or oddness of K_a , K_c , and irreps. For our $(\text{NNO})_2$ calculations, both methods agree in all cases. For example, to apply the asymmetric top symmetry rule we use the nonpolar global minimum structure which has C_{2h} symmetry (isomorphic with the PI group G_4 used in our calculation). The symmetry of $|J K_a K_c\rangle$ for the C_{2h} point group has been derived by Bunker and Jensen (Table 12-11 in Ref. 73). Assignments obtained in this way agree with those we get using method (2), from which one deduces that the rotational symmetries of the 1_{01} , 1_{11} , 1_{10} levels of the ground state are B $-$, B $-$, and A $+$, if one uses the correlation between G_4 and C_{2h} : (A $+$, B $+$, A $-$, B $-$) of the G_4 group correlate with (A $_g$, B $_u$, A $_u$, B $_g$) of the C_{2h} group, respectively. Similarly, for excited vibrational states, rovibrational level symmetries also satisfy the product rule, as shown in Table VII. Rotational constants have been obtained

for the first three vibrational states by fitting the assigned levels up to $J=3$ (Table VIII). Levels computed using the exploratory 3ZaP PES are also included in Table VIII for comparison.

Centrifugal distortion constants are not included in the fitting since the errors are small without them. The rotational constants directly obtained from the $J=1$ levels agree to better than 10^{-4} cm^{-1} with the fitted rotational constants. Therefore, rotational constants for higher vibrational states, reported in Table VII, are obtained only from the $J=1$ levels. The computed rotational constants (Table VIII, F12b) agree very well with experimental data even though the torsional and geared experimental rotational constants are for combination bands involving the in-phase ν_1 vibration mode. The levels and rotational constants calculated using the 3ZaP exploratory PES (Table VIII, 3ZaP) are in much worse agreement with experiment confirming that constructing the high-level F12b PES was necessary to describe the dynamics quantitatively.

TABLE VII. $J=1$ rotational levels (in cm^{-1}) of $(\text{NNO})_2$ for vibrational states below 99 cm^{-1} . Rotational constants are determined from the $J=1$ levels (see text).

$J=0$ level ($\nu_t, \nu_g, \nu_r, \nu_a$) (sym)	1_{01} (sym)	1_{11} (sym)	1_{10} (sym)	A	B	C
0.0000(0000)(A $+$)	0.1097(B $-$)	0.3504(B $-$)	0.3604(A $+$)	0.3005	0.0599	0.0499
25.7599(1000)(A $-$)	25.8695(B $+$)	26.1000(B $+$)	26.1093(A $-$)	0.2900	0.0595	0.0501
41.8609(0100)(B $+$)	41.9682(A $-$)	42.2244(A $-$)	42.2334(B $+$)	0.3149	0.0586	0.0487
50.7624(2000)(A $+$)	50.8717(B $-$)	51.0924(B $-$)	51.1009(A $+$)	0.2796	0.0589	0.0504
52.7591(0010)(A $+$)	52.8657(B $-$)	53.1137(B $-$)	53.1232(A $+$)	0.3061	0.0581	0.0486
65.6419(1100)(B $-$)	65.7489(A $+$)	65.9934(A $+$)	66.0026(B $-$)	0.3026	0.0581	0.0489
74.5621(3000)(A $-$)	74.6711(B $+$)	74.8836(B $+$)	74.8914(A $-$)	0.2709	0.0584	0.0506
77.2499(1010)(A $-$)	77.3561(B $+$)	77.5875(B $+$)	77.5958(A $-$)	0.2887	0.0573	0.0489
80.4367(0200)(A $+$)	80.5415(B $-$)	80.8163(B $-$)	80.8262(A $+$)	0.3321	0.0574	0.0474
86.7299(0110)(B $+$)	86.8337(A $-$)	87.1076(A $-$)	87.1172(B $+$)	0.3306	0.0567	0.0471
90.3303(2100)(B $+$)	90.4370(A $-$)	90.6695(A $-$)	90.6778(B $+$)	0.2900	0.0575	0.0492
97.5221(0001)(A $+$)	97.6300(B $-$)	97.8622(B $-$)	97.8719(A $+$)	0.2910	0.0588	0.0491
98.1581(4000)(A $+$)	98.2670(B $-$)	98.4754(B $-$)	98.4828(A $+$)	0.2666	0.0581	0.0507

TABLE VIII. Rotational constants (in cm^{-1}) of $(\text{NNO})_2$ for the three lowest vibrational states obtained by fitting to computed levels up to $J=3$.

	ν_0 ($\nu_t, \nu_g, \nu_r, \nu_a$) (sym)	A	B	C	rmsd
3ZaP	0.000(0000)(A+)	0.305 425(6)	0.057 008(10)	0.047 941(10)	8d-5
F12b	0.000(0000)(A+)	0.300 494(4)	0.059 892(6)	0.049 854(6)	5d-5
Expt. ^a	0.0 (0.0)	0.299 41	0.059 93	0.049 84	
3ZaP	25.065 (1000) (A-)	0.287 74(5)	0.056 09(4)	0.048 21(4)	4d-4
F12b	25.760 (1000) (A-)	0.289 999(2)	0.059 438(3)	0.050 116(3)	2d-5
Expt. ^b	27.3 (1.0)	0.286 41	0.059 48	0.050 09	
3ZaP	33.493(0100)(B+)	0.328 62(4)	0.056 15(6)	0.046 80(6)	5d-4
F12b	41.861(0100)(B+)	0.314 81(1)	0.058 65(2)	0.048 68(2)	1d-4
Expt. ^c	42.3 (1.0)	0.311 82	0.058 76	0.048 62	

^aReferences 8 and 11.^bReference 12.^cReference 13.

VI. SUMMARY AND CONCLUSION

We have carefully assessed the value of several *ab initio* methods for the purpose of making a 4D (intermolecular) PES for $(\text{NNO})_2$ and constructed two surfaces. Both fits were made with a refined IMLS fitting method. The highest level calculations indicate that even a qualitatively correct description of this system is remarkably challenging. The first surface was done at the CCSD(T)/3ZaP level of *ab initio* theory. Additional higher-level *ab initio* calculations performed at eight critical points (four minima and four transition structures connecting them) located on the fitted 3ZaP PES led to the conclusion that to obtain an excellent surface it was necessary to do F12b calculations. The original CCSD(T)/3ZaP was not good enough. The levels and rotational constants reported in Table VIII (for 3ZaP) are in relatively poor agreement with experiment. Furthermore, the T-shaped O-in isomer located on the 3ZaP PES was found to be spurious, while the T-shaped N-in isomer is significantly less stable at the CBS limit. The CCSD(T)-F12b method works extremely well for $(\text{NNO})_2$. Even with a double zeta basis it gives a qualitatively correct description of relative energies. CBS extrapolation was found to be robust for the F12b method with close agreement between CBS energies obtained using different extrapolation schemes. The Peterson VDZ-F12 and VTZ-F12 bases combined with the CCSD(T)-F12b method provide the two best choices balancing cost and accuracy. The CCSD(T)-F12b/VTZ-F12 method provides raw energies that differ by only 1.9 (mean) and 2.6 (rms) cm^{-1} from the best large-basis CBS estimates at the eight structures studied, making it our choice to fit a high-accuracy PES. The CCSD(T)-F12b/VTZ-F12 surface has three minima: the experimentally observed nonpolar and polar isomers as well as a T-shaped N-in isomer with only a small barrier to isomerization to the polar isomer. It provides a best estimate of the well depth of -633.43 cm^{-1} and energies of the polar and T-shaped N-in isomers of -465.20 and -421.03 cm^{-1} , respectively. Rovibrational calculations performed on the fitted F12b surface yielded vibrational frequencies and rotational constants in excellent agreement with experiment. The calculated frequencies for the torsional and gearing motions (25.76 and 41.86 cm^{-1}) are very close to the respective experimental values of 27.3(1.0) and $42.3(1.0) \text{ cm}^{-1}$. Trends

and values for rotational constants agree very well with the experiments. We have also obtained results for rovibrational levels associated with the polar and T-shaped N-in isomers. So far no experimental observation of the T-shaped isomer has been reported. The dynamics of these two isomers will be the topic of a forthcoming publication.

ACKNOWLEDGMENTS

R.D. and A.W.J. are supported by the Division of Chemical Sciences, Geosciences, and Biosciences, the Office of Basic Energy Sciences, the U.S. Department of Energy; Sandia is a multiprogram laboratory operated by Sandia Corporation, a Lockheed Martin Co., for the National Nuclear Security Administration under Contract No. DE-AC04-94-AL85000. X.-G.W. and T.C. are supported by the Natural Sciences and Engineering Research Council of Canada. Calculations were done on computers of the Réseau Québécois de Calcul de Haute Performance (RQCHP) and a computer at Queen's University purchased with money from the Canadian Foundation for Innovation.

- T. E. Gough, R. E. Miller, and G. Scoles, *J. Chem. Phys.* **69**, 1588 (1978).
- R. E. Miller, R. O. Watts, and A. Ding, *Chem. Phys.* **83**, 155 (1984).
- M. Gauthier, *J. Chem. Phys.* **88**, 5439 (1988).
- R. E. Miller and R. O. Watts, *Chem. Phys. Lett.* **105**, 409 (1984).
- Z. S. Huang and R. E. Miller, *J. Chem. Phys.* **89**, 5408 (1988).
- H.-B. Qian, W. A. Herrebout, and B. J. Howard, *Mol. Phys.* **91**, 689 (1997).
- Y. Ohshima, Y. Matsumoto, M. Takami, and K. Kuchitsu, *Chem. Phys. Lett.* **152**, 294 (1988).
- M. Dehghani, M. Afshari, Z. Abusara, N. Moazzen-Ahmadi, and A. R. W. McKellar, *J. Chem. Phys.* **126**, 164310 (2007).
- M. Dehghany, M. Afshari, R. I. Thompson, N. Moazzen-Ahmadi, and A. R. W. McKellar, *J. Mol. Spectrosc.* **252**, 1 (2008).
- N. R. Walker, A. J. Minei, S. E. Novick, and A. C. Legon, *J. Mol. Spectrosc.* **251**, 153 (2008).
- M. Dehghany, M. Afshari, Z. Abusara, C. Van Eck, and N. Moazzen-Ahmadi, *J. Mol. Spectrosc.* **247**, 123 (2008).
- M. Dehghany, M. Afshari, N. Moazzen-Ahmadi, and A. R. W. McKellar, *Phys. Chem. Chem. Phys.* **10**, 1658 (2008).
- M. Dehghany, M. Afshari, Z. Abusara, and N. Moazzen-Ahmadi, *Phys. Chem. Chem. Phys.* **11**, 7585 (2009).
- H. Valdés and J. A. Sordo, *J. Phys. Chem. A* **108**, 2062 (2004).
- G. M. Berner, A. L. L. East, M. Afshari, M. Dehghany, N. Moazzen-Ahmadi, and A. R. W. McKellar, *J. Chem. Phys.* **130**, 164305 (2009).

- ¹⁶R. A. Kendall, T. H. Dunning, Jr., and R. J. Harrison, *J. Chem. Phys.* **96**, 6796 (1992).
- ¹⁷J. N. Murrell, S. Carter, S. Frantos, P. Huxley, and A. J. C. Varandas, *Molecular Potential Energy Functions* (Wiley, Toronto, 1984).
- ¹⁸T. Hollebeek, T.-S. Ho, and H. Rabitz, *Annu. Rev. Phys. Chem.* **50**, 537 (1999).
- ¹⁹M. J. T. Jordan, K. C. Thompson, and M. A. Collins, *J. Chem. Phys.* **102**, 5647 (1995).
- ²⁰M. A. Collins, *Theor. Chem. Acc.* **108**, 313 (2002).
- ²¹S. Manzhos and T. Carrington, Jr., *J. Chem. Phys.* **125**, 084109 (2006).
- ²²B. J. Braams and J. M. Bowman, *Int. Rev. Phys. Chem.* **28**, 577 (2009).
- ²³R. Dawes, D. L. Thompson, A. F. Wagner, and M. Minkoff, *J. Chem. Phys.* **128**, 084107 (2008).
- ²⁴R. Dawes, A. Passalacqua, A. F. Wagner, T. D. Sewell, M. Minkoff, and D. L. Thompson, *J. Chem. Phys.* **130**, 144107 (2009).
- ²⁵R. Dawes, A. F. Wagner, and D. L. Thompson, *J. Phys. Chem. A* **113**, 4709 (2009).
- ²⁶J. T. Hougen and N. Ohashi, *J. Mol. Spectrosc.* **109**, 134 (1985).
- ²⁷G. W. M. Vissers, P. E. S. Wormer, and A. van der Avoird, *Phys. Chem. Chem. Phys.* **5**, 4767 (2003).
- ²⁸G. W. M. Vissers, A. Hesselmann, G. Jansen, P. E. S. Wormer, and A. van der Avoird, *J. Chem. Phys.* **122**, 054306 (2005).
- ²⁹G. S. F. Dhont, J. H. van Lenthe, G. C. Groenenboom, and A. van der Avoird, *J. Chem. Phys.* **123**, 184302 (2005).
- ³⁰A. van der Avoird, T. B. Pederson, G. S. F. Dhont, B. Fernandez, and H. Koch, *J. Chem. Phys.* **124**, 204315 (2006).
- ³¹M. H. Karimi-Jafari and A. Maghari, *J. Phys. Chem. A* **111**, 6077 (2007).
- ³²E. Anderson, Z. Bai, C. Bischof, S. Blackford, J. Demmel, J. Dongarra, J. Du Croz, A. Greenbaum, S. Hammarling, A. McKenney, and D. Sorensen, *LAPACK User's Guide*, 3rd ed. (SIAM, Philadelphia, 1999).
- ³³B. Chang, O. Akin-Ojo, R. Bukowski, and K. Szalewicz, *J. Chem. Phys.* **119**, 11654 (2003).
- ³⁴K. Raghavachari, G. W. Trucks, J. A. Pople, and M. Head-Gordon, *Chem. Phys. Lett.* **157**, 479 (1989).
- ³⁵R. J. Bartlett, J. D. Watts, S. A. Kucharski, and J. Noga, *Chem. Phys. Lett.* **165**, 513 (1990).
- ³⁶J. Gauss, W. J. Lauderdale, J. F. Stanton, J. D. Watts, and R. J. Bartlett, *Chem. Phys. Lett.* **182**, 207 (1991).
- ³⁷J. D. Watts, J. Gauss, and R. J. Bartlett, *J. Chem. Phys.* **98**, 8718 (1993).
- ³⁸MOLPRO, a package of *ab initio* programs designed by H.-J. Werner and P. J. Knowles, Version 2009.1, R. Lindh, F. R. Manby, M. Schütz *et al.*
- ³⁹T. J. Lee and P. R. Taylor, *Int. J. Quantum Chem., Symp.* **23**, 199 (1989).
- ⁴⁰D. Feller, K. A. Peterson, and T. D. Crawford, *J. Chem. Phys.* **124**, 054107 (2006).
- ⁴¹D. W. Schwenke, *J. Chem. Phys.* **122**, 014107 (2005).
- ⁴²J. G. Hill, K. A. Peterson, G. Knizia, and H.-J. Werner, *J. Chem. Phys.* **131**, 194105 (2009).
- ⁴³S. Zhong, E. C. Barnes, and G. A. Petersson, *J. Chem. Phys.* **129**, 184116 (2008).
- ⁴⁴T. B. Adler, G. Knizia, and H.-J. Werner, *J. Chem. Phys.* **127**, 221106 (2007).
- ⁴⁵K. A. Peterson, T. B. Adler, and H.-J. Werner, *J. Chem. Phys.* **128**, 084102 (2008).
- ⁴⁶X. Chapuisat and C. Iung, *Phys. Rev. A* **45**, 6217 (1992).
- ⁴⁷X.-G. Wang and T. Carrington, Jr., *J. Chem. Phys.* **115**, 9781 (2001).
- ⁴⁸M. J. Bramley and T. Carrington, Jr., *J. Chem. Phys.* **99**, 8519 (1993).
- ⁴⁹M. Mladenović, *J. Chem. Phys.* **112**, 1070 (2000).
- ⁵⁰C. Iung, F. Gatti, A. Viel, and X. Chapuisat, *Phys. Chem. Chem. Phys.* **1**, 3377 (1999).
- ⁵¹J. C. Light, I. P. Hamilton, and J. V. Lill, *J. Chem. Phys.* **82**, 1400 (1985).
- ⁵²J. C. Light and T. Carrington, Jr., *Adv. Chem. Phys.* **114**, 263 (2000).
- ⁵³Z. Bacic and J. C. Light, *Annu. Rev. Phys. Chem.* **40**, 469 (1989).
- ⁵⁴R. G. Littlejohn, M. Cargo, T. Carrington, Jr., K. A. Mitchell, and B. Poirier, *J. Chem. Phys.* **116**, 8691 (2002).
- ⁵⁵X.-G. Wang and T. Carrington, Jr., *J. Chem. Phys.* **118**, 6946 (2003).
- ⁵⁶X.-G. Wang and T. Carrington, Jr., *J. Chem. Phys.* **121**, 2937 (2004).
- ⁵⁷R. N. Zare, *Angular Momentum* (Wiley, New York, 1988).
- ⁵⁸H. Wei and T. Carrington, Jr., *J. Chem. Phys.* **97**, 3029 (1992).
- ⁵⁹J. Echave and D. C. Clary, *Chem. Phys. Lett.* **190**, 225 (1992).
- ⁶⁰X.-G. Wang and T. Carrington, Jr., *J. Chem. Phys.* **114**, 1473 (2001).
- ⁶¹R. Chen and H. Guo, *J. Chem. Phys.* **114**, 1467 (2001).
- ⁶²J. K. Cullum and R. A. Willoughby, *Lanczos Algorithms for Large Symmetric Eigenvalue Computations* (Birkhäuser, Boston, 1985).
- ⁶³M. J. Bramley, J. W. Tromp, T. Carrington, Jr., and G. C. Corey, *J. Chem. Phys.* **100**, 6175 (1994).
- ⁶⁴X.-G. Wang and T. Carrington, Jr., *J. Phys. Chem. A* **111**, 10220 (2007).
- ⁶⁵M. J. Bramley and T. Carrington, Jr., *J. Chem. Phys.* **101**, 8494 (1994).
- ⁶⁶R. Chen, G. Ma, and H. Guo, *J. Chem. Phys.* **114**, 4763 (2001).
- ⁶⁷R. Chen and H. Guo, *J. Chem. Phys.* **108**, 6068 (1998).
- ⁶⁸T. Carrington, Jr., *Encyclopedia of Computational Chemistry*, edited by P. von Ragué Schleyer (John Wiley & Sons, Chichester, UK, 1998), Vol. 5.
- ⁶⁹X.-G. Wang and T. Carrington, Jr., *J. Chem. Phys.* **117**, 6923 (2002).
- ⁷⁰X.-G. Wang, T. Carrington, Jr., J. Tang, and A. R. W. McKellar, *J. Chem. Phys.* **123**, 034301 (2005).
- ⁷¹X.-G. Wang and T. Carrington, Jr., *J. Chem. Phys.* **119**, 101 (2003).
- ⁷²R. A. Toth, *J. Opt. Soc. Am. B* **4**, 357 (1987).
- ⁷³P. R. Bunker and P. Jensen, *Molecular Symmetry and Spectroscopy*, 2nd ed. (NRC Research Press, Ottawa, 1998).